

Advanced 3D bioprinted liver models with human-induced hepatocytes for personalized toxicity screening

Yue Ma^{1*}, Runbang He^{1*}, Bo Deng¹, Miaomiao Luo¹, Wenjie Zhang¹, Lina Mao¹, Wenxiang Hu², Yilei Mao³, Huayu Yang³ and Pengyu Huang¹

Abstract

The development of advanced *in vitro* models for assessing liver toxicity and drug responses is crucial for personalized medicine and preclinical drug development. 3D bioprinting technology provides opportunities to create human liver models that are suitable for conducting high-throughput screening for liver toxicity. In this study, we fabricated a humanized liver model using human-induced hepatocytes (hiHeps) derived from human fibroblasts via a rapid and efficient reprogramming process. These hiHeps were then employed in 3D bioprinted liver models with bioink materials that closely mimic the natural extracellular matrix. The constructed humanized 3D bioprinted livers (h3DPLs) exhibited mature hepatocyte functions, including albumin expression, glycogen storage, and uptake/release of indocyanine green and acetylated low-density lipoprotein. Notably, h3DPLs demonstrated increased sensitivity to hepatotoxic agents such as acetaminophen (APAP), making them a promising platform for studying drug-induced liver injury. Furthermore, our model accurately reflected the impact of rifampin, a cytochrome P450 inducer, on CYP2E1 levels and APAP hepatotoxicity. These results highlight the potential of hiHep-based h3DPLs as a cost-effective and high-performance alternative for personalized liver toxicity screening and preclinical drug testing, paving the way for improved drug development strategies and personalized therapeutic interventions.

Keywords

Liver toxicity screening, human-induced hepatocytes, 3D bioprinting, humanized 3D bioprinted livers

Date received: 11 October 2024; accepted: 30 December 2024

¹Engineering Research Center of Pulmonary and Critical Care Medicine Technology and Device (Ministry of Education), Tianjin Institutes of Health Science, Institute of Biomedical Engineering, Chinese Academy of Medical Sciences & Peking Union Medical College, Tianjin, China

²Department of Basic Research, Guangzhou National Laboratory, Guangdong, China

³Department of Liver Surgery, Peking Union Medical College Hospital, Chinese Academy of Medical Sciences & Peking Union Medical College, Beijing, China

*These authors contributed equally to this work.

Corresponding authors:

Pengyu Huang, Engineering Research Center of Pulmonary and Critical Care Medicine Technology and Device (Ministry of Education), Tianjin Institutes of Health Science, Institute of Biomedical Engineering, Chinese Academy of Medical Sciences & Peking Union Medical College, Road Baidi, Nankai District, Tianjin 300192, China.
Email: huangpengyu@yeah.net

Huayu Yang, Department of Liver Surgery, Peking Union Medical College Hospital, Chinese Academy of Medical Sciences & Peking Union Medical College, No.1 Shuaifuyuan Wangfujing Dongcheng District, Beijing 100730, China.
Email: dolphinyahy@hotmail.com

Yue Ma, Engineering Research Center of Pulmonary and Critical Care Medicine Technology and Device (Ministry of Education), Tianjin Institutes of Health Science, Institute of Biomedical Engineering, Chinese Academy of Medical Sciences & Peking Union Medical College, Road Baidi, Nankai District, Tianjin 300192, China.
Email: mayue@bme.cams.cn



Introduction

Advancements in pharmacogenetics and pharmacogenomics, elucidating the genetic determinants influencing inter-individual variability in drug response and treatment outcomes, have significantly propelled our comprehension of the molecular underpinnings governing disease and therapeutic interventions.^{1–5} The pharmacokinetic journey of most drugs involves their transit through the liver.^{6–8} As the primary site for these crucial transformations, the liver plays a pivotal role in modulating the bioavailability and therapeutic effectiveness of various pharmaceutical agents.⁹ The development of *in vitro* liver models using human cells would be supportive to assess the liver toxicity of personalized medicine.

Three-dimensional (3D) bioprinting with cell-laden constructs, offers cells an environment emulating the extracellular matrix (ECM) and facilitating cell-cell and cell-ECM interactions, which provides a growth milieu that closely resembles that within the human body.^{9–11} Compared to emerging technologies such as organoids and organ-on-a-chip systems, 3D bioprinting enables the rapid fabrication of numerous highly consistent and complex artificial tissue or organ structures, making it a promising approach for constructing artificial liver tissues or organs *in vitro*.^{12–15} The scaffolds created by 3D bioprinting provide a cell-friendly environment, allowing for the long-term culture of bioprinted tissues.^{16,17} Moreover, the 3D environment engineered through bioprinting has the potential to enhance the specific functions of mature hepatocytes.^{18,19} This opens avenues for the creation of *in vitro* human liver models conducive to high-throughput screening for liver toxicity.^{20,21}

The quality of cell sources is paramount for creating functional 3D bioprinted tissues and organs.²² The isolation and culture of primary human hepatocytes (PHHs) have been hailed as the benchmark for constructing *in vitro* human liver models. The current culture methods for primary human hepatocytes (PHHs) face challenges in expansion. Although it is possible to isolate plenty of hepatocytes from human-derived liver tissues, maintaining liver-specific functions of PHHs through the culture process remains limited and it is difficult to harvest PHHs from patients.^{23,24} This makes it difficult to utilize as a cell source for 3D bioprinting.²⁵ Hepatocarcinoma cell lines have been applied in various studies. However, hepatocarcinoma cell lines manifest shortcomings in liver-specific functions, particularly metabolic functions.^{26–29}

Human-induced hepatocytes (hiHeps) can be generated from fibroblasts through lentiviral expression of liver-specific transcription factors,^{30,31} which exhibit functional characteristics similar to mature hepatocytes and demonstrate the ability to expand *in vitro*.³⁰ They have been utilized in genetic toxicity testing and regenerative medicine applications for a long time.^{32,33} Although the recent

advancements of stem-cell derived hepatocytes make it possible employed in 3D bioprinting,^{34–36} hiHeps offer a more cost-effective alternative.³⁷ The safety concerns of *in vivo* transplantation of hiHeps remain to be addressed and using in 3D bioprinting for drug testing would be a preliminary step. In the context of personalized medicine, the similarity ensures that the toxic reactions observed in hiHeps closely mimic those in the patient's liver, aiding in more accurate predictions and personalized treatment plans.

In this study, we employed hiHeps, derived from human fibroblasts, as the cell source to fabricate a humanized 3D bioprinted livers (h3DPLs). This method significantly improved cell viability and liver-specific functions in comparison to other existing liver models. We accomplished the development of a model to simulate drug-induced acute liver injury and conducted assessments for liver injury prevention and drug interactions using the h3DPLs. The results demonstrate that the 3D bioprinted liver models are effective and could serve as personalized platforms for thorough toxicity testing. Figure 1 illustrates the comprehensive schematic design of our proposed approach.

Materials and methods

Materials

Plasmids for molecular cloning and lentivirus production: Addgene, USA. Trizol reagent: Thermo Fisher Scientific Inc., USA. Polybrene, DMEM basic medium, PBS, sodium alginate, bovine serum albumin (BSA), and the PAS stain kit: Beijing Solarbio Science & Technology Co., Ltd., China. Human fibroblast culture medium (HFM) and hepatocyte expansion culture medium (HEM): Shanghai Weien Biotechnology Co., Ltd, China. Human fibroblasts: Peking Union Medical College Hospital. Primary human hepatocytes (PHH): LV Biotech. Collagen-I and gelatin from porcine skin: Sigma-Aldrich, USA. Matrigel: Corning Inc., USA. Rabbit anti-human albumin (Genetex), ASGPR1 (Invitrogen), and CYP2E1 (Proteintech). Goat anti-rabbit IgG Alexa Fluor® 488/568 conjugates: Thermo Fisher Scientific Inc., USA. Triton X-100 and DAPI: Sigma-Aldrich, USA. Calcein/PI cell activity and cytotoxicity detection kit, and enhanced cell count kit (eCCK-8): Beyotime Biotechnology, China. Indocyanine green and acetaminophen: Sigma-Aldrich, USA. Rifampicin: Aladdin Reagent (Shanghai) Co., Ltd, China. N-acetyl-L-cysteine and Dil-ac-LDL: Thermo Fisher Scientific Inc., USA. HiScript III RT SuperMix for qPCR, 2×Taq Master Mix (Dye Plus), and Taq Pro Universal SYBR qPCR Master Mix: Nanjing Vazyme Biotech Co., Ltd, China. Human albumin ELISA kit and human P4502E1 ELISA kit: Shanghai Fusheng Industrial Co., Ltd., China. Vitamin C, vitamin E: MedChemexpress LLC, USA.

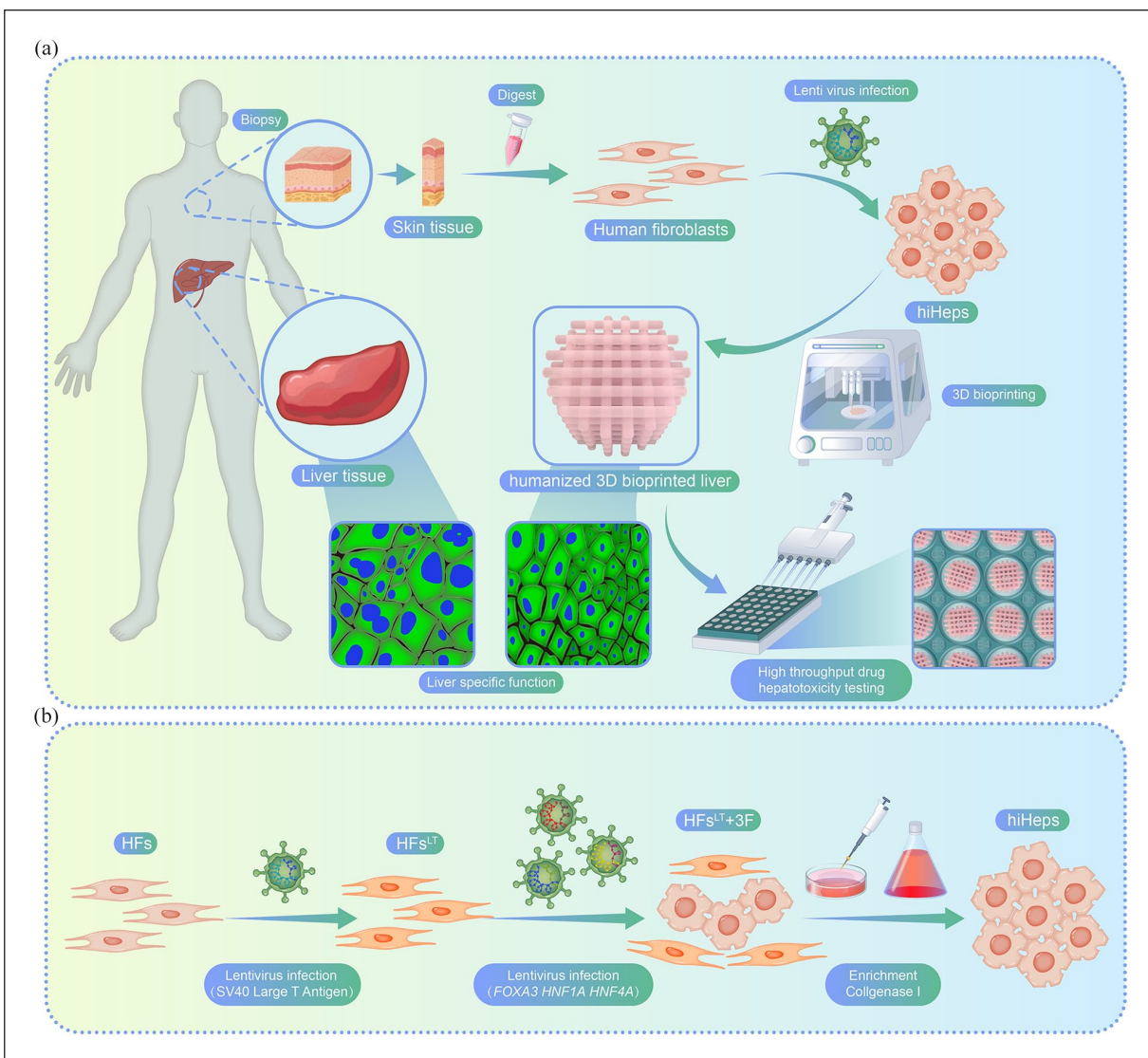


Figure 1. Schematic figure of experimental procedure and generation of hiHeps: (a) experimental procedure: the skin tissue from patients were digested fibroblasts. Fibroblasts were infected with lentivirus and transferred to related genes, leading to induction of hiHeps. hiHeps were bioprinted to fabricate h3DPLs with liver specific functions similar to human liver tissue. h3DPLs were subsequently transferred to well plates for drug hepatotoxicity testing, (b) generation of hiHeps: Human fibroblasts (HF) are first infected with lentivirus carrying SV40 Large T antigen gene. Then HF^{LT} were infected with lentivirus carrying the three transcription factors (*FOXA3*, *HNF1A*, *HNF4A*). After induction, HF^{LT}+3F were treated with collagenase I to enrich hiHeps. Abbreviations: HF: human fibroblasts; hiHeps: human induced hepatocytes.

Molecular cloning and lentivirus production

Those cDNAs of candidate genes and SV40 large T-antigen were cloned into a modified pWPI plasmid. Constructed plasmids were then introduced into 293FT cells together with packaging plasmid psPAX2 and envelop plasmid pMD2.G, in DMEM basic medium supplemented with 4 μ g/mL Polybrene for 24h, and then changed fresh DMEM basic medium for another 24h. Then the medium containing lentiviruses was collected and passed through a 0.45 μ m filter.

Cell culture

HFs were cultured at 37°C, 5% CO₂ in HFM. Human-induced hepatocytes (hiHeps) were cultured at 37°C, 5% CO₂ in HEM.

HiHep induction and enrichment

HF between passages 5 and 9 were used for hiHep production. $1.75\text{--}2 \times 10^5$ HFs were seeded on a 6 cm dish. One day later, cells were infected with lentiviruses carrying

Table 1. List of primer sequences used in amplification.

Gene	Forward (5'-3')	Reverse (5'-3')
ALB	GCCTTTGCTCAGTATCTT	AGGTTTGGGTTGTCATCT
AAT	TATGATGAAGCGTTTAGGC	CAGTAATGGACAGTTTGGGT
GJB1	ATGCTCCGACAGCGTCTC	TGCCCTCTGCTCCTCTTAC
Transferrin	TGTCTACATAGCGGGCAAGT	GTTCCAGCCAGCGGTTCT
ASGPR1	ATGACCAAGGAGTATCAAGACCT	TGAAGTTGCTGAACGTCTCTCT
GAPDH	GGAGCGAGATCCCTCCAAAAT	GGCTGTTGTCATACTTCTCATGG
AFP	ACTGAATCCAGAACAACACTGCA	TGCAGTCAATGCATCTTTCA
SOX9	GACTACACCGACCACCAGAACTCC	GTCTGCGGGATGGAAGGGA
Actin	CATGTACGTTGCTATCCAGGC	CTCCTTAATGTCACGCACGAT
CYP2E1	ATGTCTGCCCTCGGAGTCA	CGATGATGGGAAGCGGGAAA
CYP3A4	TTCAGCAAGAAGAACAAGGACAA	GGTTGAAGAAGTCTCTCTAAGC
CYP2C9	ATTTGTGTGGGAGAAGCCCT	TAGTGAAAAGATGGATAATGCCCC
CYP2C19	GCTAACAGAGGATTTGGAATCG	CCTCAATGCTCCTCTTCCC
CYP2D6	CCAGAAGGCTTTGCAGGCTTCAG	CGGCAGTGGTCAGCTAATGAC
NANOG	GATTTGTGGCCTGAAGAAA	CAGGGCTGCTCTGAATAAGC

SV40 Large T-antigen (each MOI=1) supplemented with 4 µg/mL polybrene for 24 h and then changed to fresh HFM. To generate hiHep cells, $1.0\text{--}1.5 \times 10^5$ HF^{LT} cells were seeded on a collagen I-coated 6 cm dish. One day later, cells were infected with lentiviruses carrying the three transcription factors (each MOI=1.5) supplemented with 8 µg/mL polybrene for 24 h and then changed to fresh HFM for another 24 h. The media were then changed to HEM. After the induction process was completed, cells were treated with 50 µg/mL collagenase I until fibroblasts were eliminated.

Organoids culture

Organoids were cultured in a Matrigel-based 3D system. The hiHeps cultured in collagen I-coated dishes were digested to single cells, then resuspended in ice-cold Matrigel at a density of 5×10^5 cells/mL. The mixture was plated into pre-chilled 48-well cell culture plates, polymerized at 37°C, and supplemented with HEM medium. Organoids were cultured in a humidified CO₂ incubator with medium changes every 2 days.

PCR

Total RNA was isolated by Trizol from cells, h3DPLs, and organoids. 1 µg RNA was reverse transcribed into cDNA with HiScript III RT SuperMix for qPCR (+gDNA wiper) according to manufacturer's instructions. PCR was performed with 2×Taq Master Mix (Dye Plus). Quantitative real-time PCR was performed with Taq Pro Universal SYBR qPCR Master Mix on a 7500 Fast Quantitative real-time PCR system. All q-PCR data were performed with at least two repeats. The PCR products were confirmed by proper melting curves and agarose gel electrophoresis. Primer sequences are provided in Table 1.

3D bioprinting and culture of h3DPLs

Gelatin powder was dissolved in PBS at a concentration of 12% at 70°C. Sodium alginate powder was irradiated with ultraviolet light for 40 min and then dissolved in PBS at a concentration of 4% at 70°C. To fabricate h3DPLs, hiHeps were harvested and prepared as a suspension in HEM, then mixed with 12% gelatin solution and 4% sodium alginate solution at a ratio of 2:2:1 (v/v) at 37°C, resulting in a final cell density of 1×10^6 /mL, as the bioink. The bioink was drawn into a 5 mL sterilized syringe with a 23 G needle and loaded into the 3D printer after a 15 min pre-cooling process at 4°C. Adjusting the temperatures of both the nozzle and forming chamber, then the presented model and parameters were used for bioprinting. After printing, h3DPLs were ionically crosslinked for 3 min using a 3% CaCl₂ solution.

The h3DPLs were cultured at 37°C, 5% CO₂ in HEM and medium were changed every 2 days. Crosslink using 3% CaCl₂ solution performed every 3 days.

Staining

Immunofluorescent staining: Cells and h3DPLs were fixed with 4% paraformaldehyde for 15 min at room temperature, and then washed three times with PBS. After being blocked by 3% BSA and 0.5% Triton X-100 in PBS for 60 min at room temperature, cells, and h3DPLs were incubated with primary antibodies at 4°C overnight, washed three times with PBS, and then incubated with appropriate fluorescence-conjugated secondary antibody for 2 h at room temperature in dark. Nuclei were stained with DAPI. Primary and secondary antibodies were diluted in PBS containing 3% BSA and 0.5% Triton X-100.

Indocyanine green (ICG) uptake assay: Cells and h3DPLs were changed medium with 1 mg/mL ICG and

incubated at 37°C for 1 h, followed by washing with PBS three times, then changed to fresh medium for another 4 h.

Periodic-Acid-Schiff staining and acetylated low-density lipoprotein assay: Cells and h3DPLs were stained by Periodic Acid Schiff (PAS) stain kit and Dil-ac-LDL following manufacturer's instructions.

Measurement of cell viability and proliferation

h3DPLs were treated with sodium alginate dissociation solution containing 55 mM sodium citrate, 20 mM EDTA, and 150 mM NaCl to obtain a single-cell suspension for cell counting.

Calcein/PI cell activity and cytotoxicity detection kit were used following the manufacturer's instruction for live/dead staining of cells. Quantitative analysis of live/dead staining results using ImageJ2 (Version: 2.14.0).

Cell viability was measured with an enhanced cell count kit (eCCK-8) following the manufacturer's instructions.

Evaluation of drug-induced hepatotoxic response

Acetaminophen (APAP) and N-acetyl-L-cysteine (NAC) powder were dissolved in HEM, and the pH of HEM was adjusted using a saturated NaHCO₃ solution. Rifampicin powder was dissolved in DMSO under ultrasound-assisted dissolution conditions, as a storage solution. Add the storage solution of rifampicin to HEM to account for 1% of the volume of HEM. Cells and h3DPLs were subjected to live/dead staining after 24 and 48 h of treatment, and RNA extraction and cell viability measurement were performed after 48 h of treatment. Dose-response curves were obtained using the four-parameter variable slope-fitting method (GraphPad Prism 9). Cells and h3DPLs treated with the same volume of HEM without APAP, NAC, and rifampicin were used as internal controls. Samples of each group were prepared in triplicate.

Measurement of albumin secretion and CYP2E1 activity

Albumin secretion and CYP2E1 activity of fibroblasts, hiHeps, and humanized 3D bioprinted livers were measured using ELISA kits, following the manufacturer's protocol.

Results

Generation of hiHeps with hepatocytes-specific functions

To fabricate functional humanized 3D bioprinted livers (h3DPLs), a large number of hiHeps with hepatocyte-specific functions were required. A refined method from our

previous study was employed to transdifferentiate human fibroblasts (HFs) into hiHeps.^{30,38} To enhance the proliferation capabilities, SV40 large T-antigen was transferred into HFs (Figure 1(b)). The expression of SV40 large T-antigen promotes the expansion of human fibroblasts and reaches the necessary amount for the reprogramming process. Three human transcription factors, including pioneer factors *FOXA3*, liver-enriched transcription factors *HNF1B* and *HNF4A* were carried by lentiviruses and were introduced into human fibroblasts expression of SV40 large T-antigen (HFs^{LT}). Figure 2(a) showed morphology changes of HFs^{LT} after three transcription factors were transferred. HFs^{LT} began to show epithelial characteristics and maintained proliferation capability. At day 10, most of the cells displayed an epithelial morphology that could be recognized as hiHeps. The expression of genes specific for mature hepatocytes such as *ALB*, *AAT*, *Transferrin*, *GJB1*, *ASGPR1*, *CYP2D6*, and *CYP2C19* were measured and analyzed by qPCR. Compared with human fibroblasts, hepatocyte-specific genes expression of hiHeps was close to the level of primary human hepatocytes (Figure 2(b)). To confirm the hepatocyte-specific functions of hiHeps, immunofluorescence staining of hepatocyte-specific proteins was performed in hiHeps. The results demonstrated that *ALB* and *ASGPR1* were expressed in hiHeps (Figure 2(c)), and they were not expressed in HFs (Figure S1). Moreover, key mature hepatocyte functions, including indocyanine green (ICG) uptake and release (Figure 2(d)), acetylated low-density lipoprotein (ac-LDL) uptake (Figure 2(e)), and glycogen storage (Figure 2(f)) were also verified in our hiHeps. The secretion of albumin and CYP2E1 activity of hiHeps were also measured using ELISA kits, and the results confirmed that hiHeps possess liver-specific functions (Figure 2(g and h)). By confirming the hepatocyte-specific functions at multiple levels, we have proved the successful generation of hiHeps. These expandable, functional hiHeps were subsequently used as seed cells for the 3D bioprinting of h3DPLs.

Fabrication of humanized 3D bioprinted liver (h3DPL) tissues

A gelatin and alginate-based material, modified from previous research, was used to fabricate humanized liver tissues *in vitro*.²⁶ To facilitate placement into a 48-well plate for high-throughput liver toxicity testing, the 3D bioprinted liver (h3DPL) tissues were designed cylindrically with a diameter of 10 mm and a height of 2 mm, and porous structures were fabricated to facilitate the effective exchange of substances between hiHeps and the surrounding environment. As shown in Figure 3(a), the structure of h3DPLs remained stable throughout the subsequent cultivation which confirmed the gelatin and alginate-based material was able to serve as a support system. Live/dead staining of h3DPLs demonstrated that the viability of hiHeps was maintained at a high level (Figure 3(b)).

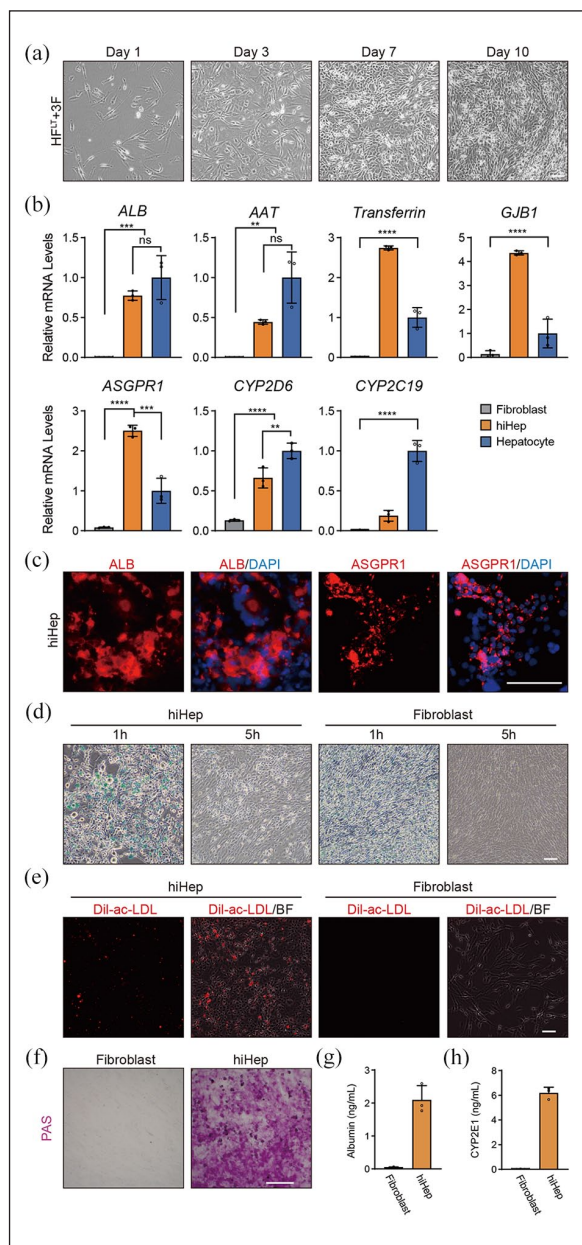


Figure 2. Generation of hiHeps with hepatocytes-specific functions: (a) HF_{st}⁺3F gradually exhibits epithelioid clones during induction process, (b) hepatic gene expression in hiHeps, (c) mature hepatic proteins albumin and ASGPR1 expression in hiHeps was determined by immunofluorescence staining, (albumin: red; ASGPR1: red; DAPI: blue) (d) indocyanine green (ICG) uptake and release in hiHeps, (green) (e) intake of acetylated low density lipoprotein labeled with the fluorescent probe 1,1'-dioctadecyl-3,3,3',3'-tetramethyl-indocarbocyanine perchlorate (Dil-ac-LDL) in hiHeps, (red) (f) glycogen storage by hiHeps was confirmed by Periodic Acid Schiff (PAS) staining. (magenta), (g) albumin secretion, (h) CYP2E1 activity. Scale bars, 100 μ m.

Densities of cells in h3DPLs after cultivation were counted in Figure 3(c). hiHeps continued proliferating in h3DPLs

and the cell density had reached a stable number of $1.74 \pm 0.06 \times 10^6$ cells/mL after 5 days of incubation. Cell viability and density in h3DPLs demonstrated that the gelatin-alginate hydrogel scaffold provided a conducive environment for hiHeps survival and proliferation.

The expression genes of h3DPLs, organoids and 2D cultured hiHeps was measured by real-time qPCR. Compared to the other two groups, the expression of mature hepatocyte-specific genes is much higher in h3DPLs (Figure 3(d)). Additionally, the percentage of cells expressing ALB in h3DPLs is also higher than in organoids (Figure 3(e)), and the cell numbers are of the same order of magnitude. Immunofluorescence staining for albumin showed that there is albumin existed in h3DPLs (Figure 3(f)). The secretion of albumin of h3DPLs and 2D-cultured hiHeps were measured using ELISA kits (Figure 3(g)). Indocyanine green (ICG) and acetylated low-density lipoprotein (ac-LDL) uptake were also maintained in h3DPLs (Figure 3(h and i)). Based on modified 3D liver bioprinting methods, we have successfully generated humanized liver tissues *in vitro* with good viability and mature hepatic functions similar to *in vivo* liver tissues. These h3DPLs will be applied for liver toxicity evaluation in the following experiments.

Acetaminophen (APAP) induced acute and chronic hepatotoxicity in h3DPLs

Acetaminophen (APAP), commonly used to treat pain and reduce fever, became widely used during the COVID-19 pandemic. However, excessive intake often leads to APAP-induced acute liver injury and is frequently employed to study drug-induced liver injury mechanisms.^{39,40} As shown in Figure 4(a), APAP is converted to the hepatotoxic N-acetyl-p-benzoquinone imine (NAPQI) by CYP2E1 enzymes in liver parenchymal cells. Glutathione binds to NAPQI, forming a conjugate that produces cysteine and mercapturic acid. However, when glutathione is depleted, NAPQI damages cellular macromolecules, leading to liver cell death. N-acetylcysteine (NAC) is a well-known antidote for APAP-induced hepatotoxicity. It is metabolized into cysteine, which replenishes glutathione levels, preventing cell death by maintaining adequate glutathione.

To investigate the toxicity response of hiHeps, live/dead staining was conducted on 2D cultured hiHeps to measure cell death after APAP treatment. As shown in Figure 4(b), there was a significant decline in viable cells as APAP treatment duration increased, indicating APAP-induced injury to hiHeps. Quantitative analysis (Figure 4(c)) revealed that the surviving cell percentage significantly dropped after 48 h of treatment, from $93.35 \pm 5.21\%$ (24 h) to $32.76 \pm 4.07\%$ (48 h). This suggests that most APAP-induced cell death occurs after 24 h, and the damage at 48 h was extensive. Therefore, subsequent experiments used a 48-h APAP treatment duration.

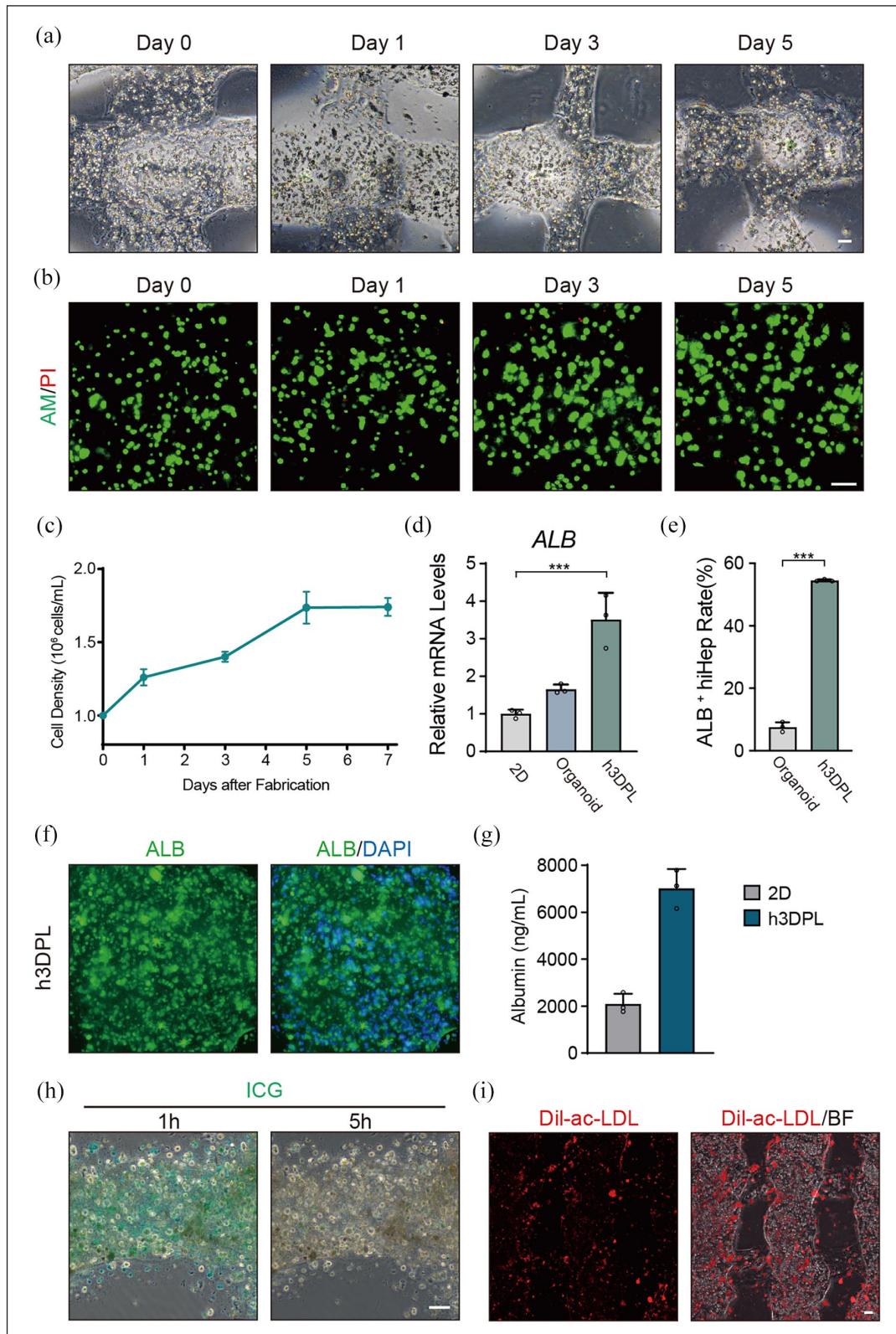


Figure 3. Fabrication of humanized 3D bioprinted liver (h3DPL) tissues: (a) bright field photos during 5 days of culture of h3DPLs, (b) images of live/dead staining during 5 days of culture of h3DPLs, (Live: green; Dead: red) (c) cell proliferation curve of hiHeps in h3DPLs, (d) hepatic gene expression in hiHeps in h3DPLs and organoids. The expression levels of the indicated genes were analyzed by qPCR. Data are normalized to hiHeps in h3DPLs, (e) the albumin positive hiHep rate in organoids and h3DPLs was calculated from the fluorescence intensity of immunofluorescence staining images using ImageJ2 (Version: 2.14.0), (f) albumin expression in hiHeps in 2D and h3DPLs was determined by immunofluorescence staining, (Green) (g) albumin secretion, (h) ICG uptake and release in hiHeps in h3DPLs, (green) (i) intake of Dil-ac-LDL in hiHeps in h3DPLs, (red) Scale bars, 100 μ m.

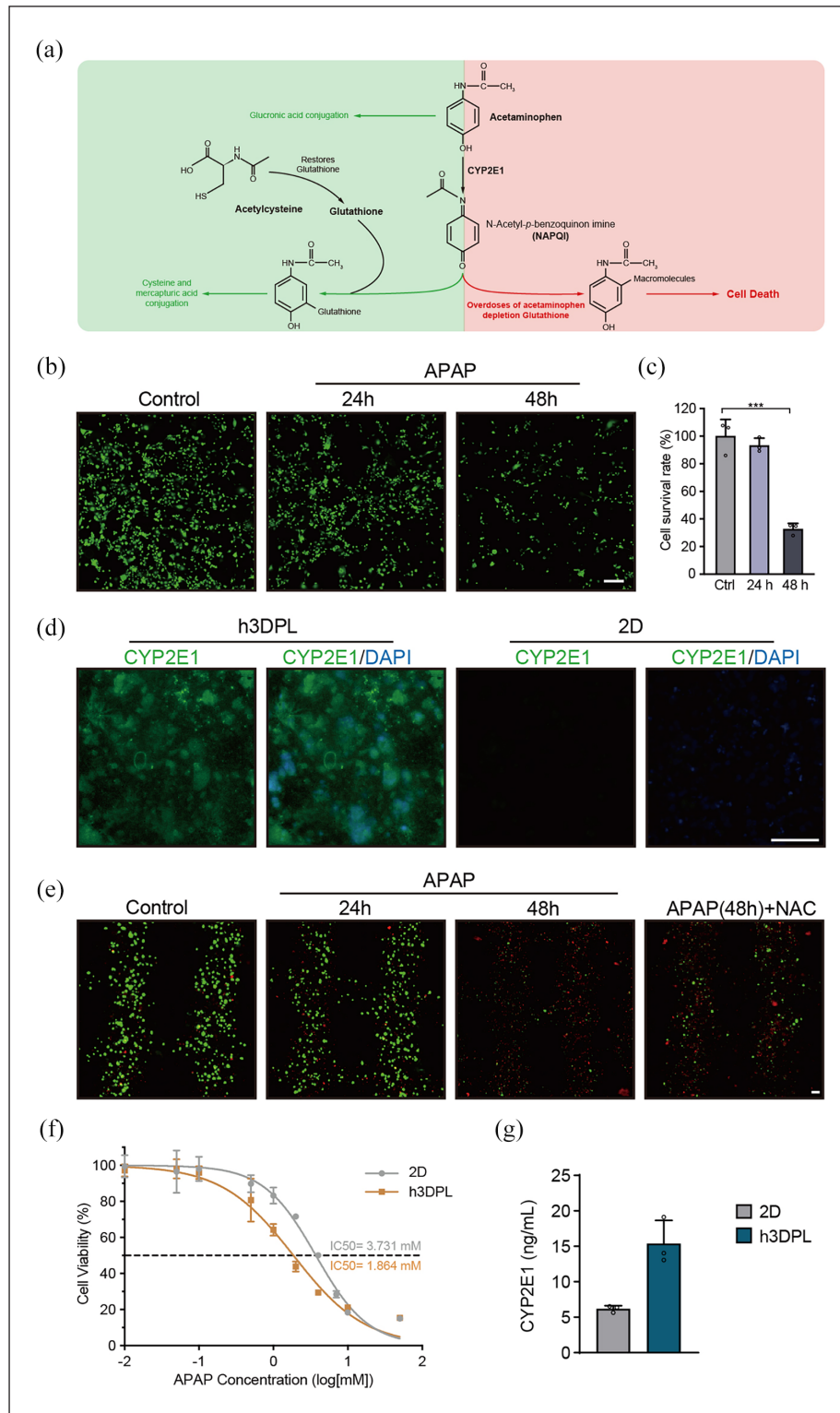


Figure 4. hiHeps in h3DPLs respond to acute hepatotoxicity caused by acetaminophen (APAP): (a) the mechanism of acute hepatotoxicity caused by APAP and prevention by N-acetylcysteine (NAC), (b) images of live cell staining of hiHeps in 2D with different APAP treatment durations under the APAP exposure of 4mM, (Green) (c) the cell survival rate of hiHeps in 2D with different APAP treatment durations was calculated from the fluorescence intensity of live cell staining images using ImageJ2 (Version: 2.14.0) (d) CYP2E1 expression in hiHeps in h3DPLs was determined by immunofluorescence staining, (Green) (e) images of live/dead staining of hiHeps in h3DPLs with different APAP treatment durations and NAC treatment under the APAP exposure of 4mM and the NAC exposure of 5mM, (Live: green; Dead: red) (f) dose-response curves of hiHeps in 2D and h3DPLs after 48 h treatment of APAP. Dose-response curves were obtained using the four-parameter variable slope-fitting method by GraphPad Prism 9, (g) CYP2E1 activity. Scale bars, 100 μ m.

Cytochrome P450 2E1 (CYP2E1) plays a critical role in drug-induced liver damage by metabolizing various medications and environmental toxins into reactive metabolites. To confirm the presence of CYP2E1 in h3DPLs, immunofluorescence staining and ELISA experiments were conducted (Figure 4(d and g)). These results demonstrated the presence of CYP2E1 in h3DPLs, suggesting their capability to respond to APAP-induced injury. Live/dead staining of h3DPLs after 5 days of cultivation showed that APAP is toxic to hiHeps within this model, leading to cell death (Figure 4(e)). Dose-response curves indicated increased sensitivity to APAP in h3DPLs, with an IC50 value of 1.864 mM, compared to a higher IC50 of 3.731 mM for hiHeps in traditional 2D culture (Figure 4(f)). Thus, h3DPLs represent a more sensitive model for studying APAP-induced acute liver injury.

We further evaluated the impact of adding N-acetylcysteine (NAC) on APAP-induced injury in our h3DPL model. The results demonstrated that NAC could mitigate the damage caused by APAP on hiHeps within h3DPLs. Cell viability analysis showed that concurrent treatment with NAC provided protective effects against excessive APAP-induced injury (Figure 5(a)). The protective effect was dose-dependent, with higher NAC concentrations offering greater protection, especially as the concentration of APAP increased. This indicates that NAC can effectively reduce APAP-induced toxicity in hiHeps when used in appropriate concentrations.

The effects of rifampin on APAP-induced acute liver injury in h3DPLs was also been explored. Rifampin, an anti-tuberculosis drug and known cytochrome P450 inducer, can elevate CYP2E1 levels in liver parenchymal cells.⁴¹ To determine whether rifampin influenced hiHeps in h3DPLs, we measured CYP2E1 gene expression using qPCR. As shown in Figure 5(b), relative mRNA levels of CYP2E1 in h3DPLs increased following rifampin treatment, with higher rifampin concentrations promoting greater CYP2E1 gene expression.

Additionally, rifampin increased the sensitivity of h3DPLs to APAP in a concentration-dependent manner (Figure 5(c)). The intensification of APAP hepatotoxicity by rifampin became more pronounced with higher APAP concentrations (Figure 5(d)). The effects of ethanol, vitamin C, and vitamin E were also tested in h3DPLs, yielding results consistent with *in vivo* observations (Figure 5(e)). These findings indicate that hiHeps within h3DPLs can replicate the hepatotoxicity and pathophysiological processes seen in human liver cells, establishing h3DPLs as a promising *in vitro* model for investigating human liver toxicity.

Discussion

We successfully developed a humanized liver model using hiHeps transdifferentiated from fibroblasts, fabricated into h3DPLs via extrusion-based 3D bioprinting. Our results

demonstrate that hiHeps exhibit key hepatocyte-specific functions, including the expression of mature liver markers and functional assays such as indocyanine green uptake, ac-LDL uptake, and glycogen storage, which are consistent with primary human hepatocytes.

The modified bioink of gelatin and sodium alginate ensured cell viability and functionality during 3D bioprinting. Gelatin supported cell growth, while alginate enabled precise deposition and rapid gelation, forming a porous structure for nutrient exchange. This bioink combination provided a stable scaffold, promoting hiHep proliferation and making it ideal for liver tissue bioprinting. Our evaluation of liver-specific functions in h3DPLs further confirmed their capability to replicate mature hepatocyte activity. The expression of key hepatocyte markers in h3DPLs was comparable to or better than that of liver organoids. Functional assays further support the maturation of hiHeps in the 3D-bioprinted model. These results suggest that the h3DPLs exhibit higher functionality and more closely mimic primary human liver cells than 2D cultures or other *in vitro* liver models.

To assess the potential of h3DPLs as a personalized liver toxicity platform, we employed APAP as a model compound to induce hepatotoxicity. The increased expression of CYP2E1 in hiHeps within the h3DPLs, compared to 2D cultures, underscores the enhanced sensitivity of this 3D model to APAP-induced liver injury. The dose-response curves further confirmed that hiHeps in h3DPLs exhibit a more pronounced sensitivity to APAP treatment, highlighting the model's potential for detecting drug-induced liver injury. The protective effect of NAC against APAP toxicity demonstrated the model's responsiveness to therapeutic interventions, further validating its use in drug testing applications.

Additionally, we explored the impact of rifampin, a CYP2E1 inducer, on APAP-induced hepatotoxicity. Rifampin significantly elevated CYP2E1 expression, increasing hiHep sensitivity to APAP in a concentration-dependent manner. Since rifampin also induces other cytochrome P450 enzymes involved in acetaminophen metabolism,⁴²⁻⁴⁵ our findings are similar to results of previous studies.^{46,47} Ethanol, vitamin C, and vitamin E effects in h3DPLs reflected *in vivo* findings. These results highlight the potential of h3DPLs to model drug-drug interactions and complex liver pathophysiology, establishing their value in liver toxicity studies.

Despite these promising results, several limitations must be addressed in future research. Incorporating non-parenchymal cells, such as stellate cells, Kupffer cells, endothelial cells, and bile duct cells, will be essential for creating a more comprehensive and physiologically relevant liver model. These cell types play critical roles in liver-specific functions and are necessary for accurately replicating the human liver microenvironment. Additionally, the introduction of vascularization, potentially through the incorporation of human umbilical vein endothelial cells (HUVECs), would enhance the delivery

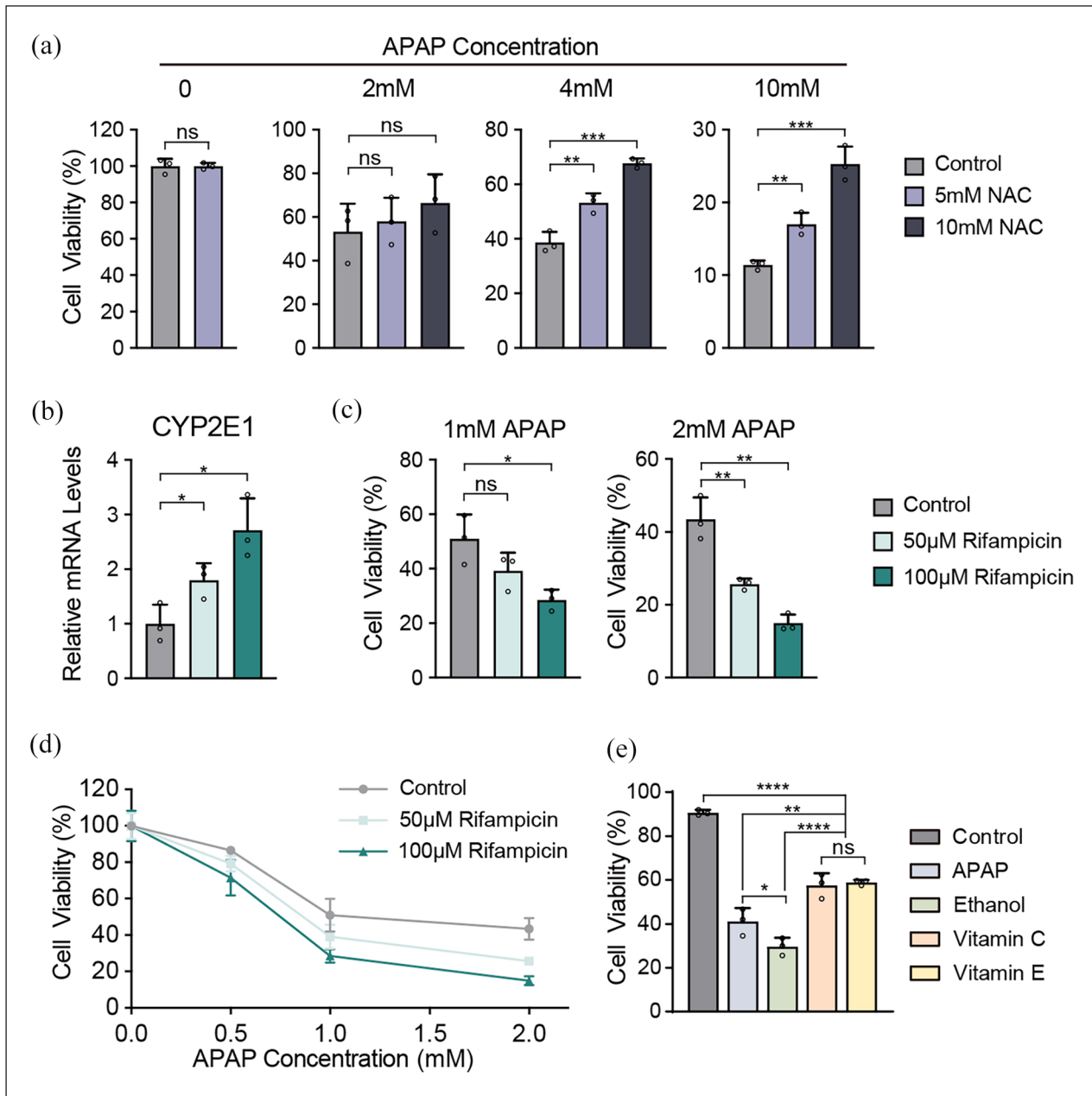


Figure 5. Prevention and drug interactions in the h3DPL hepatotoxicity model: (a) cell viability of hiHeps in h3DPLs with different NAC treatment durations under the APAP exposure of 4mM, (b) *CYP2E1* expression in hiHeps in h3DPLs with different rifampicin treatment durations. The expression levels of the indicated genes were analyzed by qPCR. Data are normalized to control (no rifampicin treatment) group, (c) cell viability of hiHeps in h3DPLs with different rifampicin treatment durations, (d) cell viability curve of hiHeps in h3DPLs with different rifampicin treatment durations, (e) cell viability of hiHeps in h3DPLs with vitamin C, vitamin E, and ethanol treatment.

of nutrients and oxygen, further improving the functionality and longevity of the bioprinted liver tissues.

Conclusion

Our study presents a robust humanized liver model utilizing hiHeps derived from human fibroblasts. h3DPLs fabricated using hiHeps and 3D bioprinting technology represent a promising platform for assessing

liver toxicity in personalized medicine. The ability to generate large numbers of hiHeps in a short period, combined with the advanced functionality of the h3DPLs, positions this model as a viable alternative to traditional 2D cultures and animal models for preclinical drug testing. Further research into the incorporation of non-parenchymal cells and vascularization will be necessary to fully realize the potential of this technology for in vitro liver modeling.

Acknowledgements

Not applicable.

Data availability statement

All datasets generated or analyzed during the current study are included in this published article and its Supplementary Information. Additional experimental details and more detailed data used or analyzed in this study are available from the corresponding author upon reasonable request.

Declaration of conflicting interests

The author(s) declared no potential conflicts of interest with respect to the research, authorship, and/or publication of this article.

Funding

The author(s) disclosed receipt of the following financial support for the research, authorship, and/or publication of this article: P.H. is funded by the Ministry of Science and Technology of China (MOST: 2024YFA1107700), CAMS Innovation Fund for Medical Sciences (2021-I2M-1-058, 2022-I2M-2-003, and 2023-I2M-2-008), the Fundamental Research Funds for the Central Universities (grant numbers 2021-RC310-004 and 2023-PT310-05), Tianjin Natural Science Foundation for Distinguished Young Scholars (21JCJJC00030), Beijing-Tianjin-Hebei Basic Research Cooperation Special Project (22JCZXC00200), and the Tianjin Municipal Science and Technology Commission (grant number 23ZXRKSY00010). H.Y. is funded by National Natural Science Foundation of China (grant number 32271470), National High Level Hospital Clinical Research Funding (2022-PUMCH-B-034).

Ethical approval statement


Written informed consent was obtained from all the patients prior to tissue acquisition. The study was conducted in accordance with recognized ethical guidelines and received approval from the Ethics Review Committee of Peking Union Medical College Hospital (Approval No. I-23PJ156).

Consent for publication

Not applicable.

ORCID iD

Yue Ma  <https://orcid.org/0000-0002-8924-2860>

Pengyu Huang  <https://orcid.org/0000-0001-8394-7280>

Supplemental material

Supplemental material for this article is available online.

References

1. Donnette M, Hamimed M, Ciccolini J, et al. Pharmacokinetics and pharmacogenetics of liposomal cytarabine in AML patients treated with CPX-351. *J Control Release* 2021; 338: 244–252.
2. Leopold JA and Loscalzo J. Emerging role of precision medicine in cardiovascular disease. *Circ Res* 2018; 122(9): 1302–1315.
3. Bianco C, Casirati E, Malvestiti F, et al. Genetic predisposition similarities between NASH and ASH: identification of new therapeutic targets. *JHEP Rep* 2021; 3(3): 100284.
4. Ghouse J, Sveinbjörnsson G, Vujkovic M, et al. Integrative common and rare variant analyses provide insights into the genetic architecture of liver cirrhosis. *Nat Genet* 2024: 1–11.
5. Zhou Y, Tremmel R, Schaeffeler E, et al. Challenges and opportunities associated with rare-variant pharmacogenomics. *Trends Pharmacol Sci* 2022; 43(10): 852–865.
6. Almazroo OA, Miah MK and Venkataramanan R. Drug metabolism in the liver. *Clin Liver Dis* 2017; 21(1): 1–20.
7. Ganesh S, Almazroo OA, Tevar A, et al. Drug metabolism, drug interactions, and drug-induced liver injury in living donor liver transplant patients. *Clin Liver Dis* 2017; 21(1): 181–196.
8. Olsen L, Oostenbrink C and Jorgensen FS. Prediction of cytochrome P450 mediated metabolism. *Adv Drug Deliv Rev* 2015; 86: 61–71.
9. Jammalamadaka U and Tappa K. Recent advances in biomaterials for 3D printing and tissue engineering. *J Funct Biomater* 2018; 9(1): 22.
10. Salaris F and Rosa A. Construction of 3D in vitro models by bioprinting human pluripotent stem cells: challenges and opportunities. *Brain Res* 2019; 1723: 146393.
11. Atala A. Introduction: 3D printing for biomaterials. *Chem Rev* 2020; 120(19): 10545–10546.
12. Zhu W, Qu X, Zhu J, et al. Direct 3D bioprinting of prevascularized tissue constructs with complex microarchitecture. *Biomaterials* 2017; 124: 106–115.
13. Brancato V, Oliveira JM, Correlo VM, et al. Could 3D models of cancer enhance drug screening? *Biomaterials* 2020; 232: 119744.
14. Kim GA, Ginga NJ and Takayama S. Integration of sensors in gastrointestinal organoid culture for biological analysis. *Cell Mol Gastroenterol Hepatol* 2018; 6(1): 123–131.
15. Deng B, Ma Y, Huang J, et al. Revitalizing liver function in mice with liver failure through transplantation of 3D-bioprinted liver with expanded primary hepatocytes. *Sci Adv* 2024; 10(23): eado1550.
16. Bhatt SS, Krishna Kumar J, Laya S, et al. Scaffold-mediated liver regeneration: a comprehensive exploration of current advances. *J Tissue Eng* 2024; 15: 20417314241286092.
17. Xue T, Wei H, Li F, et al. MicroRNA-modified DNA hexahedron-induced hepatocyte-like cells integrating 3D printed scaffold for acute liver failure therapy. *Adv Funct Mater* 2024; 34(38): 2402339.
18. Zhang J, Chen X, Chai Y, et al. 3D printing of a vascularized mini-liver based on the size-dependent functional enhancements of cell spheroids for rescue of liver failure. *Adv Sci* 2024; 11(17): 2309899.
19. Zhang J, Chan HF, Wang H, et al. Stem cell therapy and tissue engineering strategies using cell aggregates and decellularized scaffolds for the rescue of liver failure. *J Tissue Eng* 2021; 12: 2041731420986711.
20. Ma L, Wu Y, Li Y, et al. Current advances on 3D-bioprinted liver tissue models. *Adv Healthc Mater* 2020; 9(24): e2001517.
21. Jin Y, Zhang J, Chen X, et al. 3D printing incorporating gold nanozymes with mesenchymal stem cell-derived hepatic

- spheroids for acute liver failure treatment. *Biomaterials* 2025; 315: 122895.
22. Ma Y, Deng B, He R, et al. Advancements of 3D bioprinting in regenerative medicine: exploring cell sources for organ fabrication. *Heliyon* 2024; 10(3): e24593.
 23. Kim Y, Kang K, Lee SB, et al. Small molecule-mediated reprogramming of human hepatocytes into bipotent progenitor cells. *J Hepatol* 2019; 70(1): 97–107.
 24. Zhang K, Zhang L, Liu W, et al. In vitro expansion of primary human hepatocytes with efficient liver repopulation capacity. *Cell Stem Cell* 2018; 23(6): 806–819.
 25. Nguyen DG, Funk J, Robbins JB, et al. Bioprinted 3D primary liver tissues allow assessment of organ-level response to clinical drug induced toxicity in vitro. *PLoS One* 2016; 11(7): e0158674.
 26. Yang H, Sun L, Pang Y, et al. Three-dimensional bioprinted hepatorganoids prolong survival of mice with liver failure. *Gut* 2021; 70(3): 567–574.
 27. Jeon H, Kang K, Park SA, et al. Generation of multilayered 3D structures of HepG2 cells using a bio-printing technique. *Gut Liver* 2017; 11(1): 121–128.
 28. He J, Wang J, Pang Y, et al. Bioprinting of a hepatic tissue model using human-induced pluripotent stem cell-derived hepatocytes for drug-induced hepatotoxicity evaluation. *Int J Bioprint* 2022; 8(3): 581.
 29. Sun L, Yang H, Wang Y, et al. Application of a 3D bioprinted hepatocellular carcinoma cell model in antitumor drug research. *Front Oncol* 2020; 10: 878.
 30. Huang P, Zhang L, Gao Y, et al. Direct reprogramming of human fibroblasts to functional and expandable hepatocytes. *Cell Stem Cell* 2014; 14(3): 370–384.
 31. Garcia-Llorens G, Martinez-Sena T, Pareja E, et al. A robust reprogramming strategy for generating hepatocyte-like cells usable in pharmaco-toxicological studies. *Stem Cell Res Ther* 2023; 14(1): 94.
 32. Wang Y, Su W, Wang L, et al. Paper supported long-term 3D liver co-culture model for the assessment of hepatotoxic drugs. *Toxicol Res (Camb)* 2018; 7(1): 13–21.
 33. Wang Y, Zheng Q, Sun Z, et al. Reversal of liver failure using a bioartificial liver device implanted with clinical-grade human-induced hepatocytes. *Cell Stem Cell* 2023; 30(5): 617–631.
 34. Park E, Kim HK, Jee J, et al. Development of organoid-based drug metabolism model. *Toxicol Appl Pharmacol* 2019; 385: 114790.
 35. Bell CC, Lauschke VM, Vorrink SU, et al. Transcriptional, functional, and mechanistic comparisons of stem cell-derived hepatocytes, HepaRG cells, and three-dimensional human hepatocyte spheroids as predictive in vitro systems for drug-induced liver injury. *Drug Metab Dispos* 2017; 45(4): 419–429.
 36. Bouwmeester MC, Tao Y, Proença S, et al. Drug metabolism of hepatocyte-like organoids and their applicability in in vitro toxicity testing. *Molecules* 2023; 28(2): 621.
 37. Shi XL, Gao Y, Yan Y, et al. Improved survival of porcine acute liver failure by a bioartificial liver device implanted with induced human functional hepatocytes. *Cell Res* 2016; 26(2): 206–216.
 38. Huang P, Sun L, Zhang L, et al. Conversion of fibroblasts to hepatocytes in vitro. *Methods Mol Biol* 2019; 1905: 93–101.
 39. Heard KJ. Acetylcysteine for acetaminophen poisoning. *New Eng J Med* 2008; 359(3): 285–292.
 40. Yoon E, Babar A, Choudhary M, et al. Acetaminophen-induced hepatotoxicity: a comprehensive update. *J Clin Transl Hepatol* 2016; 4(2): 131–142.
 41. Lancaster EM, Hiatt JR and Zarrinpar A. Acetaminophen hepatotoxicity: an updated review. *Arch Toxicol* 2015; 89(2): 193–199.
 42. Thummel KE, Lee CA, Kunze KL, et al. Oxidation of acetaminophen to N-acetyl-p-aminobenzoquinone imine by human CYP3A4. *Biochem Pharmacol* 1993; 45(8): 1563–1569.
 43. Laine JE, Auriola S, Pasanen M, et al. Acetaminophen bioactivation by human cytochrome P450 enzymes and animal microsomes. *Xenobiotica* 2009; 39(1): 11–21.
 44. Patten CJ, Thomas PE, Guy RL, et al. Cytochrome P450 enzymes involved in acetaminophen activation by rat and human liver microsomes and their kinetics. *Chem Res Toxicol* 1993; 6(4): 511–518.
 45. Bolleddula J, Gopalakrishnan S, Hu P, et al. Alternatives to rifampicin: a review and perspectives on the choice of strong CYP3A inducers for clinical drug–drug interaction studies. *Clin Transl Sci* 2022; 15(9): 2075–2095.
 46. He M, Zhang S, Jiao Y, et al. Effects and mechanisms of rifampin on hepatotoxicity of acetaminophen in mice. *Food Chem Toxicol* 2012; 50(9): 3142–3149.
 47. Khanal S, Ghimire P and Dharmoon AS. Liver injury during treatment with rifampicin, vancomycin, and acetaminophen. *Am J Ther* 2018; 25(6): e735–e737.